nature protocols

https://doi.org/10.1038/s41596-026-01407-0

Protocol

Check for updates

Direct printing of metasurfaces using formulated optical materials

In the format provided by the authors and unedited

Table of contents

Supplementary Note 1. XRD analysis of TiO_2 nanoPER

To characterize the TiO_2 nanoparticles and TiO_2 nanoPER, X-ray diffraction (XRD) analysis is performed. XRD is a technique in which X-rays are diffracted by a sample, producing a diffraction angle–intensity spectrum that reveals its internal crystalline structure. Since the wavelength of X-rays (≈0.5–2.5 Å) is comparable to the size of atomic spacings, the technique enables detection of crystalline phases within the material. As shown by the JCPDS reference card No. 21-1272, a strong diffraction peak corresponding to the (101) plane of anatase TiO_2 appears near $2\theta \approx 25.3°$. This characteristic peak is observed in both the TiO_2 NP dispersion and the TiO_2 nanoPER, while no peaks associated with rutile or brookite are detected, confirming the high phase purity of anatase TiO_2 within the nanoPER. Furthermore, the preservation of this diffraction signature after UV curing indicates that the intrinsic NP crystallinity remains unchanged during nanoimprinting.

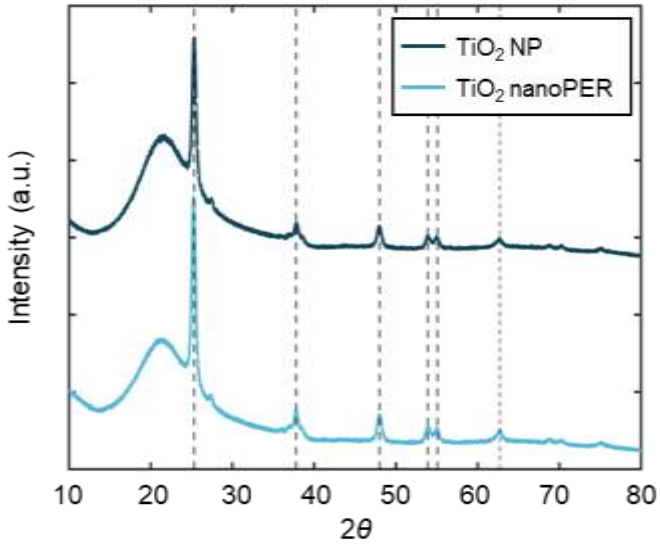

Supplementary Figure 1. X-ray diffraction (XRD) patterns of TiO_2 nanoparticle (NPs) and TiO_2 NP-embedded resin (nanoPER). Dashed lines mark the standard peak positions for anatase (JCPDS No. 21-1272). The patterns are plotted as a function of the diffraction angle 2θ, where 2θ is twice the incident angle θ defined in Bragg's law.

Supplementary Note 2. Effect of meta-atom bending angle on optical performance

To evaluate the mechanical deformation tolerance of nanoPER-based metasurfaces, we analyze how the bending angle of individual meta-atoms affects their optical performance. Two representative TiO_2 nanoPER meta-atom geometries are considered: (i) height (h) = 1000 nm, period (p) = 400 nm, length (l) = 350 nm, width (w) = 100 nm, and (ii) h = 1000 nm, p = 600 nm, l = 540 nm, w = 75 nm. Electric-field propagation simulations are performed while gradually increasing the bending angle of each structure. For both geometries, the conversion efficiency remains relatively stable for bending angles up to approximately 15°. However, the phase response shows noticeable variation as the bending angle increases. When the bending angle exceeds ~20°, clear degradation in optical performance is observed, including reduced conversion efficiency and significant phase distortion. The electric field distributions (E_x, E_y) shown in **Supplementary Figs. 2b** and **2d** indicate that, when the bending angle exceeds 20°, the structure can no longer function effectively as the intended meta-atom. Notably, within a bending angle of ≤10°, the phase variation remains very small (~0.1), indicating that the designed phase response is largely preserved. These findings suggest that nanoPER-based metasurfaces can tolerate small bending deformations (≤10°) without substantial degradation in optical performance. However, larger bending angles can significantly modify the phase distribution and may degrade the performance of phase-sensitive metasurface devices such as metalenses or holograms.

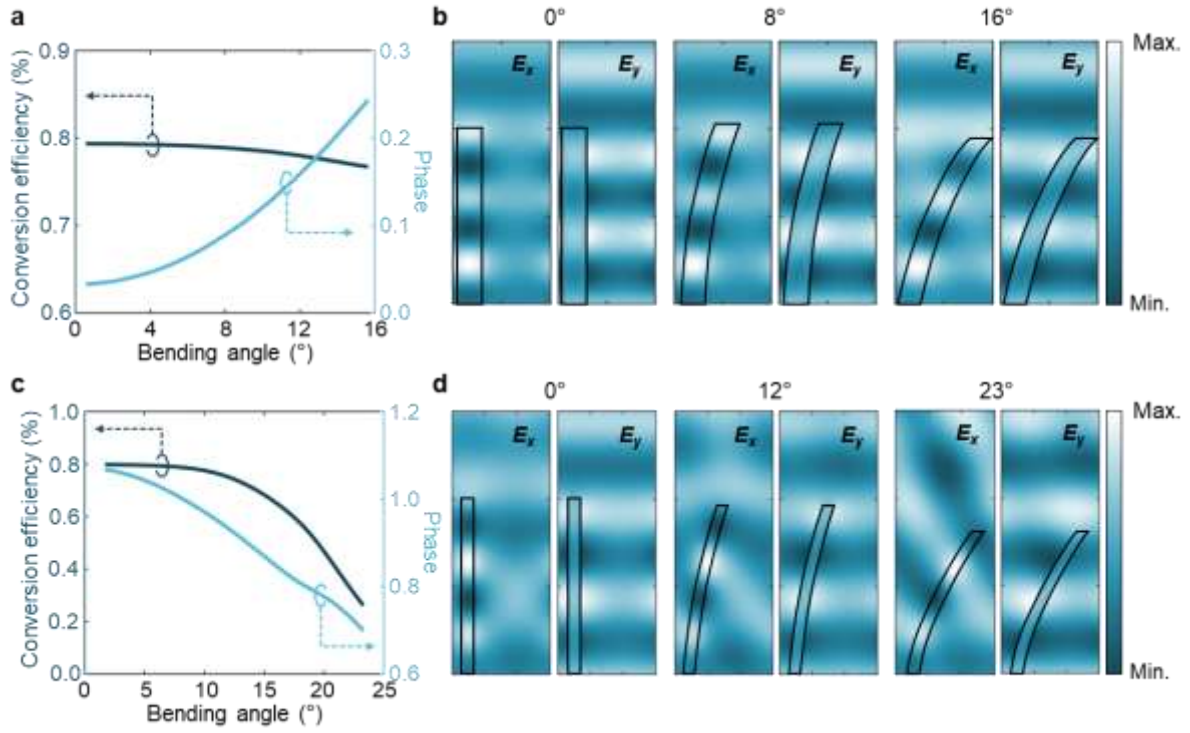

Supplementary Figure 2. a,**b**, Conversion efficiency and phase response (**a**), and simulated electric field distributions (**b**) of a meta-atom with geometry (h = 1000 nm; p = 400 nm; l = 350 nm, w = 100 nm) under increasing bending angles. **c**,**d**, Conversion efficiency and phase response (**c**), and simulated electric field distributions (**d**) and phase response of a meta-atom with geometry (h = 1000 nm; p = 600 nm; l = 540 nm; w = 75 nm) under increasing bending angles.

Supplementary Note 3. Measurement of UV intensity at different positions inside the nanoimprinter

The UV lamp used in the nanoimprinter exhibits a point-source emission profile, resulting in a gradual decrease in irradiance toward the edges of the exposure area. Nevertheless, the measured intensity at all positions exceeds 0.8 $mW \cdot cm^{-2}$ at 365 nm, which is sufficient for uniform and complete curing of the resin. Therefore, as long as the minimum exposure time of 10 minutes is maintained, spatial variations in irradiance do not adversely affect the curing process. UV intensity measurements are performed using a power meter (Thorlabs, PM100D2) in combination with a photodiode power sensor (Thorlabs, S120VC). The UV power at each position is first recorded and then divided by the sensor's active area to obtain the irradiance.

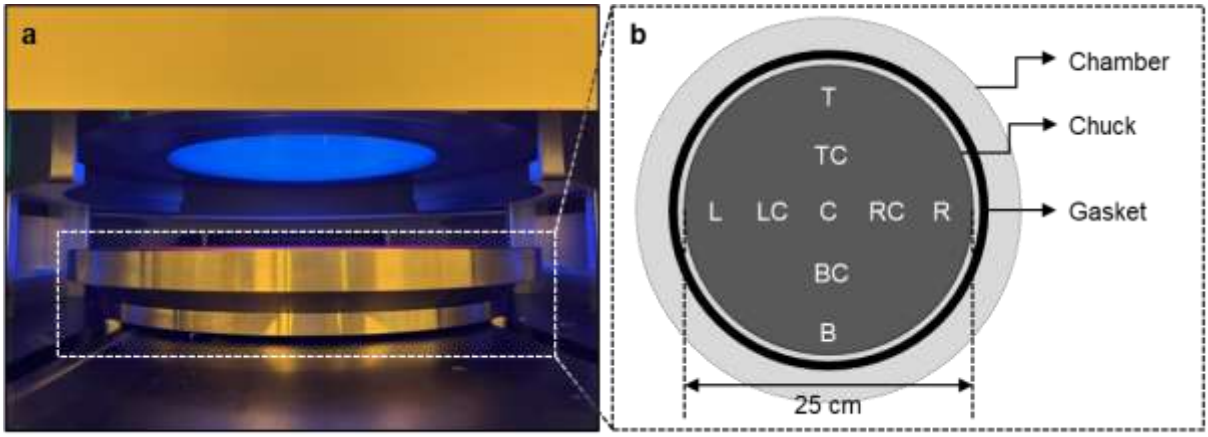

c

-	L	LC	C	RC	R	T	TC	BC	B
UV intensity (mW/cm^2)	0.87	1.85	2.85	1.81	0.9	0.85	1.85	1.12	0.79

Supplementary Figure 3. a, Photograph of UV irradiation inside the nanoimprinter. **b**, Schematic illustration of the nanoimprinter chamber showing the measurement positions: left (L), left-center (LC), center (C), right-center (RC), right (R), top (T), top-center (TC), bottom-center (BC), and bottom (B). **c**, Table summarizing the measured UV intensities at each location.

Supplementary Note 4. Evaluation of pressure uniformity during nanoimprinting

To evaluate the pressure uniformity of the nanoimprinting process, samples are placed simultaneously at five locations on the nanoimprinter chuck—top (T), bottom (B), left (L), right (R), and center (C)—and imprinted under identical conditions (5 bar pressure and 15 min UV irradiation). SEM images from each region confirm that the replicated TiO_2 nanoPER-based structures maintain consistent feature fidelity across the entire chuck area.

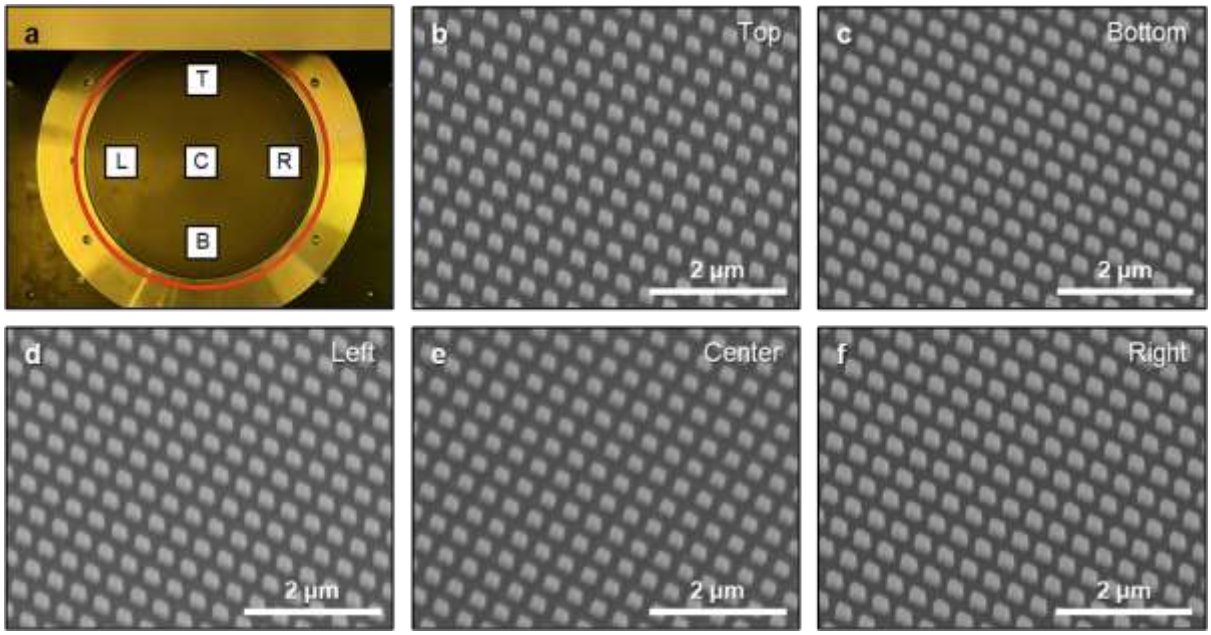

Supplementary Figure 4. a, Photograph of the nanoimprinter chuck showing the five sampling positions. **b–f**, Scanning electron microscope (SEM) images of TiO_2 nanoPER-based structures obtained from the top, bottom, left, center, and right regions, respectively, demonstrating uniform pattern replication across the imprint area.

Supplementary Note 5. Reproducibility of the TiO_2 nanoPER-based imprinting

To evaluate the reproducibility of the nanoimprinting process, ten consecutive nanoimprints are performed using the same master mold. Across all ten runs, the replicated TiO_2 nanoPER-based structures exhibit consistent pattern quality and uniformity, confirming the high reproducibility of our imprinting procedure.

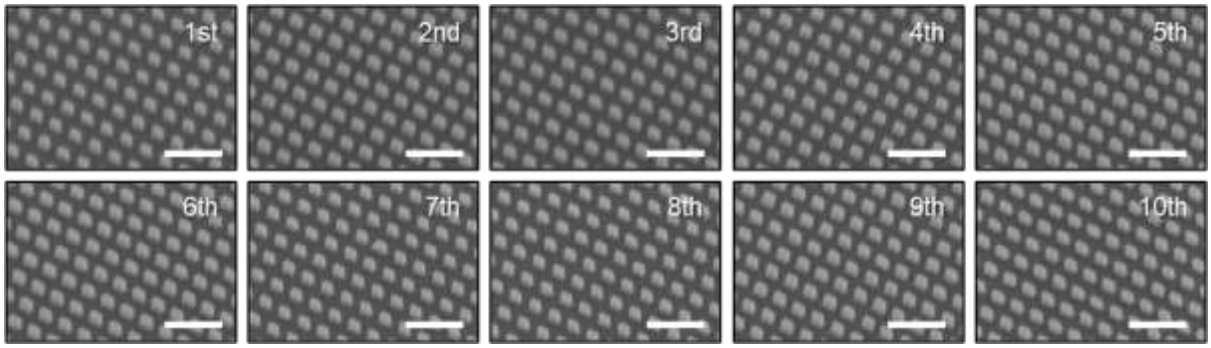

Supplementary Figure 5. Scanning electron microscope (SEM) images of TiO_2 nanoPER-based structures replicated over ten consecutive nanoimprinting cycles using the same master mold. Scale bars: 1 μm.

Supplementary Note 6. Imprinting TiO_2 nanoPER-based metasurfaces onto a flexible film

To demonstrate compatibility with non-planar and flexible substrates, the TiO_2 nanoPER-based metasurfaces are transferred onto a polyethylene terephthalate (PET) film using the same imprinting protocol described in the main text. The transferred metasurfaces remain conformally attached to the flexible substrate without any cracking or delamination, even when the film is bent (**Supplementary Fig. 6a**). SEM images obtained from multiple regions of the flexible film (**Supplementary Figs. 6b, c**) show that the nanostructures preserve their morphology, height, and lateral dimensions, indicating that the nanoPER material and imprinting process support high-fidelity pattern replication on deformable substrates.

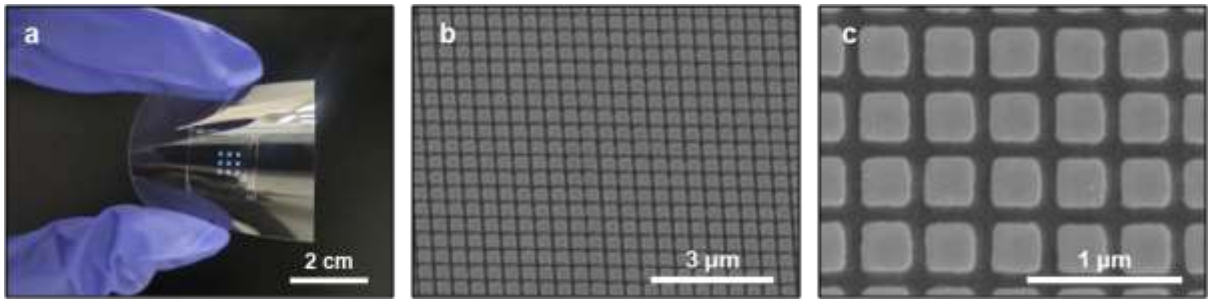

Supplementary Figure 6. a, Photograph of TiO_2 nanoPER-based metasurfaces transferred onto a flexible polyethylene terephthalate (PET) film. **b,c**, Scanning electron microscope (SEM) images of the TiO_2 nanoPER-based structures on the PET film.